Supporting Information

Hadid et al. 10.1073/pnas.1222588110

SI Materials and Methods

DNA Extraction. DNA was extracted from skin tissue samples taken from animals anesthetized with standard phenol-chloroform (1). In addition, other DNA was extracted from fecal samples with QIAamp DNA Stool Mini Kit (QIAGEN), which is painless for animals. All animals were treated in accordance with University of Haifa guidelines.

The sequences of part of the *control region* (600 bp) of the *Spalax* mtDNA were obtained by PCR amplification [annealing temperature (TA), Ta = 59 °C] with primers 15320F (5′-tggtcttgtaaaccagaaatgg) and 93R (5′-aataaggccaggaccaaacc) and sequencing with the primer 16087R (5′-ccacctgttggagatgtgtg). The mtDNA gene *ATP6* was sequenced following PCR amplification (Ta = 59 °C) with primers 7701F (5′-gcttttagcgctagcctttt) and 9437R (5′-ttgttctgatctgtttgattgga) and sequencing with the primer 8648R (5′-ccatgggcttgggtttactat). The sequencing of the entire mtDNA genome was performed with 66 primers that are available from the authors upon request. The sequencing followed the previously published mtDNA complete sequence of *Spalax judaei* (2). All DNA sequences reported herein were deposited in the GenBank database under accession numbers CR (FJ436196,-200–203,-205, -211,-212; FJ477341) and *ATP6* (FJ477338,-40,-42,-46; JN575736, -49,-59). DNA sequencing was done on an Applied Biosystems 3130xl DNA Analyzer following the ABI Prism Dye Terminator cycle-sequencing protocols (www.appliedbiosystems.com).

Bioinformatics Software and Statistical Analyses. The obtained sequences were corrected and aligned using the software Sequencher 4.7 (Gene Codes Corp.). After alignment, maximum likelihood phylograms and chronograms were constructed using PhyML_3 (3). The optimal substitution model and the test for selection was identified with Hyphy software (4). To choose the optimal model, we used the Akaike Information Criterion (5). The most probable model of molecular evolution identified in the concatenated DNA fragments was HKY85. This model assumes that the rates of substitution differ between each of the nucleotides (6). Population statistics were conducted on mtDNA haplotypes sequences. The program DNAsp (7) was used to estimate haplotype diversity (*Hd*), nucleotide diversity (*Pi*), population differentiation (*Fst*), and gene flow (*Nm*). The presence of recombinations in the dataset was tested by means of 14 relatively powerful tests available in RDP3 (8).The software STRUCTURE (9) was used to test for the presence of population structure, the most likely number of populations with distinct haplotype frequencies (K), and the estimation of Dirichlet admixture coefficient α. In this program we used the 'admixture model' based on empirical experience with the dataset, and set up the burn-in period of 200,000 iterations and 800,000 iterations of a Markov chain Monte Carlo simulation. We also used the LOCPRIOR model to estimate *r* that parameterizes the amount of information carried by the locations [Alma (ALM,)/Kerem Ben Zimra (KBZ)]. Values of *r* near 1 or < 1 indicate that the locations are informative (9). Strong assignment of some individuals to one or the other population and the presence of the asymmetric proportions assigned to each mtDNA cluster are regarded as indicating that the obtained population structure represents the real population structure (9). Because it was shown that the modal value of the distribution of the ΔK is located at the real K (10), we used this parameter to determine the number of clusters present. The differences between haplotype frequencies in the pooled sample and pairwise comparisons of haplotype frequencies were tested by using the binomial probabilities (11). To measure concordance in a categorical setting, we used Cohen's Unweighted Kappa (K) (12). Overall significance was estimated by the Fisher's combined probability test (Fisher's X^2) (13). Two-tailed tests were used for testing, and the level of significance was set as $\alpha = 0.05$. The exceptions were binomial test (Table S3) and Fisher's χ^2. In the Fisher's χ^2, α was adjusted for the approximate false-discovery rate, $\alpha_s = \alpha(k + 1)/(2k)$, to account for potentially too-small *P* values.

Daily Activity Patterns. The animals that were radio-tracked were captured in both soil types [basalt (ALM) and chalk (KBZ)] in the microsite in December 2011. Eight animals (six females, two males) from KBZ and 12 animals (six females, six males) from ALM were anesthetized by ketamine and xylazine and were fitted with radio collars (a brass collar and a Pip transmitter; Biotrack Ltd.). The weight of the radio collar was less than 5% of body mass of the smallest radio-tracked animal under study. All animals were released back into their own burrow system within 24 h after capture. Radio-tracking was performed in one continuous 72-h session (January 19–21, 2012). We used an IC-R20 receiver (Icom America Inc.) and a three-element handheld Yagi antenna to locate positions of the mole rats. The animals were radio-tracked in rotation with an interval of 60 min between consecutive fixes of the same individual. Radio-tracking started with an observer checking for the animal's presence in the nest (i.e., the single place where it was encountered most frequently) from a distance of 2 m. If the animal was not found in the nest, it was approached carefully and fixed from a distance of 1–4 m. To determine outside-nest activity, each radio fix was designated as either inside or outside the nest. Based on our previous radio-tracking studies of subterranean rodents, we estimated the accuracy of fixes at 0.5 m; thus, all fixes within a 0.5-m radius of the nest were treated as inside the nest (14, 15). Subsequently, all radio fixes of each individual (72 radio fixes per individual) were grouped into twelve 2-h blocks, and the proportion of fixes outside the nest was determined for each of the blocks. Differences in proportions of outside-nest activity in KBZ and ALM mole rats were compared by analysis of covariance (ANCOVA) in STATISTICA 10 (16) with tested factors of habitat, sex, and their interaction. The size of individual home-range (assessed as a minimum area of the convex polygons encompassing all radio fixes of the given animal) was treated as a covariable. Proportions of outside-nest activity were Arcsine transformed before the analysis.

Oxygen Consumption Experimental System and Procedure. ***Animals.*** Five mole rats from the basalt population (three males and two females), weighing 166 ± 22 g, and six animals from the chalk population (four males and two females), weighing 205 ± 27g, were used.

Experimental chamber. The experimental chamber is a metal, double-walled chamber (25 × 20 × 12 cm, total volume 6.0 L). One wall and the top cover, which could be opened, are made of Plexiglas to allow observation of the animal. Thermoregulated water (C/H Temperature Controller Bath and Circulator 2067; Forma Scientific) at a temperature of 29.5° [thermoneutral for the mole rats (17)] was recirculated through the double wall to control the ambient temperature. The flow of gas through the chamber was controlled by needle valves and a flow-meter, which was calibrated using a flow calibrator (DryCAL Model DCL-M; Bios International Corp.). Airflow of 680 mL/min was driven through the chamber. The outgoing gas exited via a canister for absorbance of water vapor (Drierite; Vacuumed) and a tube that

fed the oxygen analyzer with a bypass tube bubbling through water to ensure that the sample driven by the oxygen meter was from the gas exiting the experimental cage. The O_2 analyzer (model 17518; Vacuumed) was calibrated before each test. Oxygen consumption was calculated from a multiplication of airflow and the inflow–outflow difference in oxygen concentration and is given as milliliters of O_2 [standard temperature and pressure, dry (STPD) correction factor]$\cdot h^{-1} \cdot g^{-1}$.

Flora and Vegetation. The vegetation in the ALM–KBZ site is a typical Mediterranean community. One can assume that without long-term grazing in this site, a Mediterranean scrub dominated by *Quercus calliprinos* trees would have evolved. As a consequence of grazing, one can find batha areas dominated by *Poterium* shrublets and by annual and perennial herbaceous plants. Both geological formations are rich in herbaceous ora but differ in vegetation. The basalt area is dominated by ephemeral herbaceous ora, covering 84% (March) to 63% (May) of the area. Sustained shrublets cover only 1–2% of the area; these plants are scattered *Poterium* shrublets that probably are a result of mass effect from the chalky area. The chalky area looks more arid; *Poterium* shrublets cover 30% (March) to 55% (May) of the area, and ephemeral plants (most of which, in contrast to plants in the basalt area, are annuals) cover 25% (March) to 5% (May) of the area. Two botanical surveys took place in early spring and late spring (March–May, 2012) and covered most of the local ora. Seventy-six different plant species were found in the basalt area, and 69 were found in the chalky part. Only thirty-two species (28%), often differing in abundance, were found in both areas (Table S5).

Although these samplings are on a small scale, we can conclude that the basalts are dominated by a combination of more temperate Mediterranean elements (e.g., *Dactylis glomerata*, several *Trifolium* species, and *Acanthus syriacus*) and the chalky area by more arid ones (e.g., *Sacropoterium spinosum*, *Ceratocephala falcata*, and *Teucrium polium*). It is interesting that *Iris histrio* was found only in the chalks at the site, although it is found in basalts of the Golan Heights. Two other bulbs show a differential pattern between the soils—*Crocus hyemalis* in chalks and *Crocus aleppicus* in basalt—indicating that other taxa also speciate between chalk and basalt.

1. Sambrook J, Fritsh EMT (1989) *Molecular Cloning: A Laboratory Manual* (Cold Spring Harbor Laboratory, Cold Spring Harbor, NY).
2. Reyes A, et al. (2004) Congruent mammalian trees from mitochondrial and nuclear genes using Bayesian methods. *Mol Biol Evol* 21(2):397–403.
3. Guindon S, Gascuel O (2003) A simple, fast, and accurate algorithm to estimate large phylogenies by maximum likelihood. *Syst Biol* 52(5):696–704.
4. Pond SLK, Frost SDW, Muse SV (2005) HyPhy: Hypothesis testing using phylogenies. *Bioinformatics* 21(5):676–679.
5. Akaike H (1973) Maximum likelihood identification of Gaussian autoregressive moving average models. *Biometrika* 60(2):255–265.
6. Hasegawa M, Kishino HH, Yano T (1985) Dating of the human-ape splitting by a molecular clock of mitochondrial DNA. *J Mol Evol* 22(2):160–174.
7. Librado P, Rozas J (2009) DnaSP v5: A software for comprehensive analysis of DNA polymorphism data. *Bioinformatics* 25(11):1451–1452.
8. Martin DP, et al. (2010) RDP3: A flexible and fast computer program for analyzing recombination. *Bioinformatics* 26(12):2462–2463.
9. Pritchard JK, Wen X, Falush D (2010) *Documentation for Structure Software Version 2.3* (Univ of Chicago, Chicago).
10. Evanno G, Regnaut S, Goudet J (2005) Detecting the number of clusters of individuals using the software STRUCTURE: A simulation study. *Mol Ecol* 14(8):2611–2620.
11. Lowry R (2011) Binomial Probabilities: VassarStats: Website for Statistical Computations. Available at http://faculty.vassar.edu/lowry/VassarStats.html. Accessed December 2012.
12. Lowry R (2011) *Kappa as Measure Concordance in Categorical Sorting* (http://faculty.vassar.edu/lowry/VassarStats.html).
13. Fisher RA (1925) *Statistical Methods for Research Workers* (Oliver and Boyd, Edinburgh), 1st Ed.
14. Šklíba J, Šumbera R, Chitaukali WN, Burda H (2007) Determinants of daily activity patterns in a free-living afrotropical solitary subterranean rodent. *J Mammal* 88(4):1009–1016.
15. Šklíba J, Šumbera R, Chitaukali WN, Burda H (2009) Home-range dynamics in a solitary subterranean rodent. *Ethology* 115(3):217–226.
16. StatSoft (2011) STATISTICA (data analysis software system), version 10. Available at: www.statsoft.com.
17. Arieli R, AR A, Shkolnik A (1977) Metabolic responses of a fossorial rodent (*Spalax ehrenbergi*) to simulated burrow conditions. *Physiol Zool* 50(1):61–75.

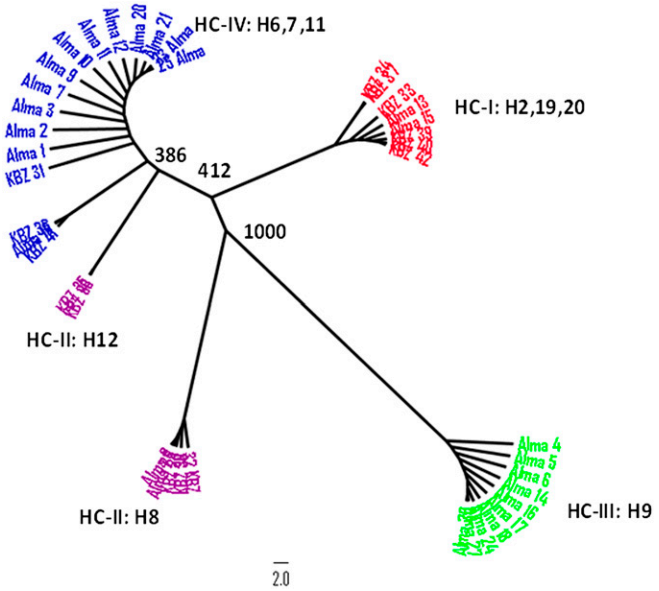

Fig. S1. A maximum likelihood-based phylogenetic tree of the four identified mtDNA haplotype clusters in the AlM–KBZ microsite. The bootstrap values are based on 1,000 bootstrap cycles.

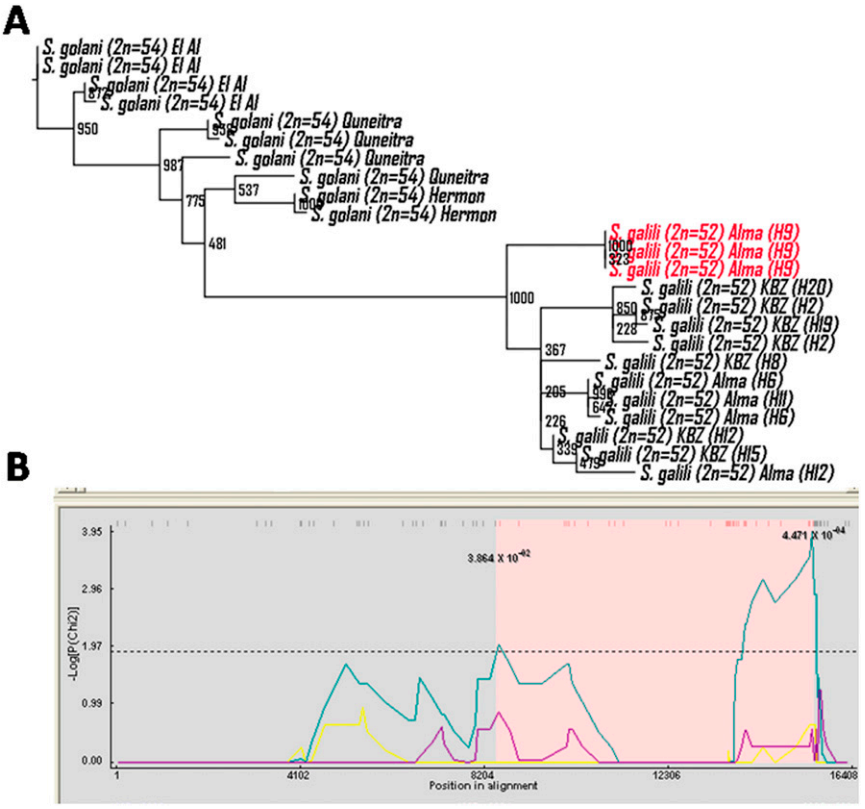

Fig. S2. (*A*) Maximum likelihood-based phylogenetic tree of the identified mtDNA haplotypes (*ATP6* and *D-loop* sequences) in Israeli blind mole rat populations ($2n$ = 52, 54). The H9 haplotype is shown in red. The bootstrap values are based on 1,000 bootstrap cycles. (*B*) Graphical results obtained by the recombination detection program Chimaera included in RDP Parental genotypes of the identified recombinant are: 2095 × 2094, Break points are at positions 15 and 405 on the sequence. The significant recombination ($P = 3.4 \times 10^{-2}$) is in pink with the significance levels given for beginning and end break points. The *x*-axis designates the position of recombinant on the alignment, and the *y*-axis designates the probability of the recombinant event. The dashed line indicates the border of the given significant level. The results obtained by Chimaera are supported by significant values in the following four other recombination detection tests: Probability ($P = 5.0 \times$ 10-6), Genconv ($P = 9.1 \times 10^{-2}$), SiScan ($P = 1.0 \times 10^{-13}$), 3s ($P = 2.3 \times 10^{-2}$). The original sequences are accessible in GenBank (access numbers JN571129–JN571132).

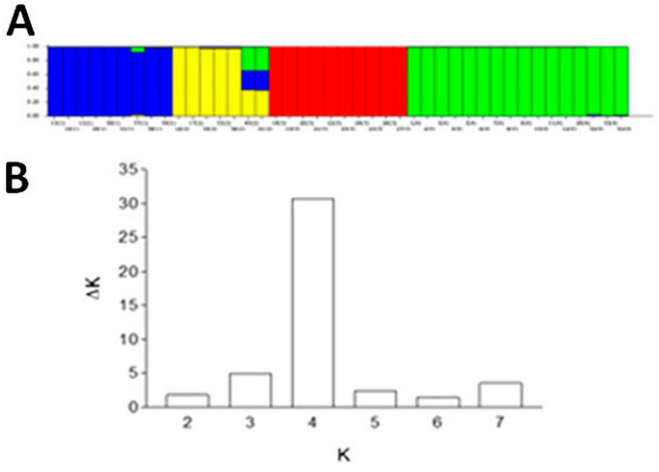

Fig. S3. (*A*) Summary plot showing admixture proportions between the four haplotypes clusters (blue, HCI; yellow, HCII; red, HCIII; green, HCIV). Each individual is represented by a single vertical line broken into K-colored segments, with lengths proportional to each of the K-inferred clusters. (*B*) The graph shows four populations (K = 4) as the most probable outcome of the structure analysis.

Table S1. Sampled specimens, their taxonomic identification, laboratory serial numbers, locality of their origin, number of chromosomes, sex, and GenBank reference numbers for the two submitted sequences

Sample no./species	Serial no.	Locality	2n*/sex	*ATP6*	*D-loop*
1. *S. golani*	411	El_Al	54/♂	FJ477334/	AJ440429
2. S. galili	1009	Dalton	52/♂	JN575733	FJ436209
3. S. galili	1018	Rihaniya	52/♂	FJ477341	FJ436206
4. S. galili	1017	Rihaniya	52/♀	FJ477347	FJ436199
5. S. galili	1015	Rihaniya	52/♂	FJ477341	FJ436206
6. S. galili	1025	Rihaniya	52/♂	JN575735	FJ436201
7. S. galili	2096	KBZ	52/♀	JN575736	FJ436205
8. S. golani	274	El_Al	54/♂	JN575746	JN599174
9. S. galili	2092	KBZ	52/♀	JN575749	FJ436211
10. S. galili	2108	KBZ	52/♀	FJ477342	FJ436196
11. S. galili	1003	Dalton	52/♀	JN575750	FJ436197
12. S. galili	1022	Rihaniya	52/♀	FJ477345	FJ436204
13. S. golani	318	El_Al	54/♂	FJ477337	AJ440427
14. S. golani	429	Hermon	54/♀	JN575754	AJ440434
15. S. golani	314	Quneitra	54/♀	FJ477335	AJ440437
16. S. galili	2095	Alma	52/♀	FJ477338	FJ436203
17. S. golani	292	Quneitra	54/♂	FJ477336	AJ440435
18. S. galili	2084	Alma	52/♂	FJ477346	FJ436200
19. S. galili	2119	Dalton	52/♀	FJ477348	FJ436213
20. S. galili	1005	KBZ	52/♀	FJ477339	FJ436208
21. S. golani	290	Quneitra	54/♀	JN575756	JN599173
22. S. galili	1061	Dalton	52/♂	FJ477344	FJ436207
23. S. galili	2103	Dalton	52/♂	JN575757	FJ436214
24. S. galili	1062	Dalton	52/♂	JN575758	FJ436198
25. S. galili	2093	KBZ	52/♂	JN575759	FJ436212
26. S. golani	279	Hermon	54/♀	JN575760	AJ440433
27. S. galili	2112	Dalton	52/♀	FJ477343	FJ436195
28. S. galili	1083	Alma	52/♂	FJ477338	FJ436203
29. S. galili	2085	KBZ	52/♀	FJ477340	FJ436202

Table S2. Sample specifications of collected specimens of *Spalax galili* from ALM basalt and KBZ chalk in the Upper Eastern Galilee Mountains, used for studying mtDNA *ATP6* and *control region* variability

No./code	Sex	Locality	Coordinates	H	HC	Pi
1. 1034*	♀	ALM	33°02′30″N, 35°29′12″E	6	IV	0.993–1.0
2. 1035	♀	ALM	33°02′30″N, 35°29′13″E	6	IV	0.993–1.0
3. 1036	♀	ALM	33°02′34″N, 35°29′20″E	6	IV	0.993–1.0
4. 1037	♀	ALM	33°02′33″N, 35°29′18″E	9	III	0.992–1.0
5. 1039	♀	ALM	33°02′33″N, 35°29′19″E	9	III	0.992–1.0
6. 1040	♂	ALM	33°02′34″N, 35°29′17″E	9	III	0.992–1.0
7. 1041	♀	ALM	33°02′33″N, 35°29′19″E	6	IV	0.993–1.0
8. 1044	♂	ALM	33°02′31″N, 35°29′17″E	8	II	0.978–1.0
9. 1046	♀	ALM	33°02′32″N, 35°29′15″E	6	IV	0.993–1.0
10. 1047	♀	ALM	33°02′35″N, 35°29′22″E	6	IV	0.993–1.0
11. 1048	♀	ALM	33°02′32″N, 35°29′15″E	6	IV	0.993–1.0
12. 1051	♀	ALM	33°02′31″N, 35°29′13″E	6	IV	0.993–1.0
13. 1065	♀	ALM	33°02′31″N, 35°29′14″E	2	I	0.985–1.0
14. 1066	♀	ALM	33°02′33″N, 35°29′18″E	9	III	0.992–1.0
15. 1067*	♀	ALM	33°02′35″N, 35°29′22″E	2	I	0.985–1.0
16. 1068	♂	ALM	33°02′31″N, 35°29′15″E	9	III	0.992–1.0
17. 1069	♀	ALM	33°02′32″N, 35°29′18″E	9	III	0.992–1.0
18. 1071	♀	ALM	33°02′33″N, 35°29′18″E	9	III	0.992–1.0
19. 1072	♀	ALM	33°02′31″N, 35°29′14″E	11	IV	0.984–1.0
20. 1073	♀	ALM	—	6	IV	0.993–1.0
21. 1074	♀	ALM	33°02′34″N, 35°29′22″E	6	IV	0.993–1.0
22. 1075	♀	ALM	33°02′33″N, 35°29′24″E	8	II	0.978–1.0
23. 1076	♀	ALM	33°02′30″N, 35°29′19″E	6	IV	0.993–1.0
24. 1083	♂	ALM	33°02′36″N, 35°29′19″E	9	III	0.992–1.0
25. 2084	♂	ALM	—	6	IV	0.993–1.0
26. 2089	♂	ALM	—	2	I	0.985–1.0
27. 2095*	♀	ALM	33°02′36″N, 35°29′18″E	9	III	0.992–1.0
28. 881	♀	ALM	—	9	III	0.992–1.0
29. 2085	♀	KBZ	33°02′28″N, 35°29′12″E	8	II	0.919–1.0
30. 2086	♂	KBZ	33°02′27″N, 35°29′15″E	8	II	0.919–1.0
31. 2087	♀	KBZ	—	6	IV	0.925–1.0
32. 2088	♀	KBZ	33°02′29″N, 35°29′09″E	8	II	0.919–1.0
33. 2092	♀	KBZ	33°02′29″N, 35°29′07″E	19	I	0.562–1.0
34. 2093	♂	KBZ	33°02′31″N, 35°29′13″E	20	I	0.785–1.0
35. 2094*	♀	KBZ	33°02′29″N, 35°29′11″E	12	II	0.268–0.994
36. 2096	♀	KBZ	—	11	IV	0.887–1.0
37. 2097	♀	KBZ	33°02′31″N, 35°29′12″E	20	I	0.785–1.0
38. 2100	♂	KBZ	33°02′30″N, 35°29′12″E	12	II	0.268–0.994
39. 2108	♀	KBZ	33°02′28″N, 35°29′07″E	2	I	0.942–1.0
40. 2123	♀	KBZ	33°02′31″N, 35°29′10″E	2	I	0.942–1.0
41. 2124	♂	KBZ	33°02′30″N, 35°29′08″E	7	IV	0.820–1.0
42. 2125	♂	KBZ	33°02′29″N, 35°29′10″E	2	I	0.942–1.0

ALM, Alma, basalt soil; KBZ, Kerem Ben Zimra, chalk, H, haplotype; HC, H cluster, *Pi*, probability interval that the specimen belongs to the inferred cluster, —, missing data.
*Samples 1034 (H6), 2095 (H9), 2094 (H12), and 1067 (H2) were sequenced for their whole mitochondrial DNA genome (16,474 bp).

Table S3. Population-genetic characteristics of mole rat populations from areas with basalt (ALM) and chalk (KBZ) soils estimated from concatenated *D-loop* and *ATP6* fragments

Locality	Sample size	HC: Hp(N_i)
ALM	28	**HC-I**: H2 (3); **HC-II**: H8 (2)·, **HC-III**: H9 (10), **HC-IV**: H6 (12); H11 (1)
KBZ	14	**HC-I**: H2 (3), H19 (1), H20 (2); **HC-II**: H8 (3), H12 (2); **HC-IV**: H6 (1)·, H7 (1), H11 (1)
ALM × KBZ	42	H2, H7, $H6^{0.038}$, H8, $H9^{0.017}$, H11, H12, H19, H20

Parameters inside parentheses indicate the sample size of specific haplotypes. *P* values, given in superscript after the haplotype numbers, indicate the significance of differences in haplotype abundance in samples tested by the binomial test. HC, haplotype cluster; Hp, haplotype number; Ni, number of haplotypes. HC are marked by bold.

Table S4. Resting oxygen consumption in $mL \cdot h^{-1} \cdot g^{-1}$ of mole rats from ALM–KBZ microsite

Chalk				Basalt			
5 min	20 min	Weight, g	Serial no.	5 min	20 min	Weight, g	Serial no.
0.73	0.8	243	2121	0.94	0.99	147	2248
0.67	0.71	229	2226	1.1	1.16	186	2258
0.84	0.92.	217	2150	1.4	1.42	167	2237
1.07	1.12	225	2086	1.67	1.7	140	1073
0.82	0.9	181	2219	1.34	1.38	189	2217
0.76	0.86	172	2209				

Table S5. Plant species found in Alma basalt, in Kerem Ben Zimra chalk, and in both soil types

Chalk	Chalk and basalt	Basalt
Aegilops triuncialis	*Aegilops ovata*	*Acanthus syriacus*
Ajuga chia	*Anagallis arvensis*	*Aegilops peregrina*
Alyssum simplex	*Anemone coronaria*	*Alcea sp*
Anthemis cornucopiae	*Anthemis palestina*	*Allium daninianum*
Asphodelus aestivus	*Avena sterilis*	*Alopecurus myosuroides*
Asteriscus spinosus	*Biscutella didyma*	*Alopecurus utriculatus*
Astragalus palaestinus	*Bromus scoparius*	*Bromus alopecuros*
Bromus fasciculatus	*Carlina hispanica*	*Bromus lanceolatus*
Bromus tectorum	*Carthamus tenuis*	*Bupleurum nudicaulis*
Calendula arvensis	*Centaurea iberica*	*Capsella bursa-pastoris*
Carlina curetum	*Cichorium pumilum*	*Carthamus glaucus*
Ceratocephala falcata	*Crepis aspera*	*Cerastium glomeratum*
Clypeola jonthlaspi	*Dactylis glomerata*	*Crepis sancta*
Crocus hyemalis	*Erodium cicutarium*	*Crithopsis delileana*
Daucus bicolor	*Eryngium creticum*	*Crocus aleppicus*
Erodium malacoides	*Erysimum crassipes*	*Crupina crupinastrum*
Erophila verna	*Filago contracta*	*Dianthus strictus*
Euphorbia helioscopia	*Hedypnois rhagadioloides*	*Echinops adenocaulos*
Filago pyramidata	*Hypericum triquetrifolium*	*Echium glomeratum*
Geranium tuberosum	*Lolium perenne*	*Geranium molle*
Linum strictum	*Medicago minima*	*Geropogon hybridus*
Lomelosia palaestina	*Medicago polymorpha*	*Hirschfeldia incana*
Muscari parviflorum	*Moraea sisyrinchium*	*Hordeum bulbosum*
Origanum syriacum	*Onobrychis squarrosa*	*Hordeum spontaneum*
Paronychia argentea	*Ononis spinosa*	*Hymenocarpos circinnatus*
Polygonum equisetiforme	*Poa bulbosa*	*Lagoecia cuminoides*
Pterocephalus brevis	*Ranunculus millefolius*	*Lamium amplexicaulis*
Ranunculus asiaticus	*Sarcopoterium spinosum*	*Linum pubescens*
Rhagadiolus stellatus	*Thlaspi perfoliatum*	*Medicago rugosa*
Rostraria cristata	*Tolpis virgata*	*Notobasis syriaca*
Senecio vernalis	*Torilis leptophylla*	*Silybum marianum*
Teucrium polium	*Torilis tenella*	*Sinapis arvensis*
Trifolium scabrum		*Stellaria pallida*
Trifolium subterraneum		*Trifolium argutum*
Trigonella monantha		*Trifolium echinatum*
Veronica syriaca		*Trifolium eriophyllum*
Vicia peregrina		*Trifolium israeliticum*
		Trifolium physodes
		Trifolium pilulare
		Trifolium resupinatum
		Trifolium stellatum
		Trigonella berythea
		Velezia rigida
		Verbascum gaillardotii